On modelling of laser assisted machining: forward and inverse problems for heat placement control

Zhendong Shang[a,b], Zhirong Liao[a,*], Jon Ander Sarasua[c], John Billingham[d], Dragos Axinte[a**]

(a) Machining and Condition Monitoring Group, Faculty of Engineering, University of Nottingham, NG7 2RD, UK
(b) School of Mechatronics Engineering, Harbin Institute of Technology, Harbin 150001, China
(c) IK4-TEKNIKER, Polo Tecnológico de Eibar, c/Iñaki Goenaga 5, Eibar, Guipuzcoa, Spain
(d) School of Mathematical Sciences, Faculty of Science, University of Nottingham, NG7 2RD, UK

Abstract

Laser assisted machining (LAM) is one of the most efficient ways to improve the machinability of difficult-to-cut materials (e.g. Nickel-based superalloys). In the conventional LAM process, the laser beam is focused ahead of the cutting area at a fixed location, which leads to a series of restrictions, e.g. small heating area and non-uniform heat distribution due to the limitation of beam size and energy distribution. In this paper, a novel spatially and temporally (S&T) controlled laser heating method was proposed, in which a large area can be heated up with a small laser spot by controlling the beam scanning, i.e., laser power, path and speed of scanning. The laser configuration for the prescribed HAZ (heat affected zone) was achieved by solving the inverse problem where the laser power together with either laser path or laser speed were optimised to achieve a particular temperature distribution in the chip to be removed by the following milling cutter. The proposed S&T laser heating method was thoroughly validated both for the forward and, the more important, inverse heating models by performing extensive temperature experiments by both infrared thermal camera and thermocouple array and further verified by laser assisted milling (LAMill) tests of Inconel 718 for large widths of cuts. The results showed that by applying path-optimised LAMill based on the inverse solution of the thermal problem, the peak and mean principal cutting forces were reduced by 55% and 47.8% respectively compared with the conventional dry milling process while the surface roughness improved by at least 14%. Moreover, after controlling the HAZ using the inverse thermal problem, a microstructure analysis of the machined surface showed that the proposed laser heating method avoids overheating of the workpiece below the planned depth of cut for the milling operation.

Keywords:

Laser assisted machining, inverse problem, thermal model, Nickel alloy

Nomenclature

a_b, the acceleration of the laser spot, unit $\mathrm{m/s^2}$;
c, the heat capacity of the workpiece material, unit J/(kg K);
C, the cost function;
d_{bt}, the minimum distance from cutting tool profile to the laser beam edging, unit m;
f_y, feed rate of the cutting process, unit m/s;
k, the thermal conductivity of the workpiece material, unit W/(m K);
m, the minimum laser trajectory overlap amount along the feed direction;
M, the number of mesh nodes of the discretised cutting cross section;
P, power of the laser system, unit W;
q''', heat source term for the laser spot, unit $\mathrm{W/m^2}$;
q_0, heat flux strength of heat source, unit $\mathrm{W/m^2}$;
r_{bx}, r_{by}, laser spot radius along x and y direction, unit m;
R_b, effective cutting radius, unit m;
R_t, the radius of the cutting tool, unit m;
t, time, unit s;
T_b, laser scanning period, unit s;
v_b, scanning speed of the laser beam, unit m/s;
α, thermal diffusivity, unit $\mathrm{m^2/s}$;
δ, the Dirac delta function;
η, laser heat absorption ratio by the workpiece material;
θ, temperature, unit °C;
θ_0, the targeted temperature, unit °C;
ρ, density of the workpiece material, unit kg/m^3.

1 Introduction

Due to their superior thermo-mechanic characteristics such as high-temperature strength and corrosion resistance, nowadays more and more high-strength advanced engineering materials (e.g. Ni/Ti based superalloys [1, 2], ceramics matrix composite [3]) are being developed and used in industries for higher product performance, especially in the aerospace industry. They are however often difficult-to-cut by conventional machining methods [4] because of their physical and mechanical properties such as low thermal conductivity [5, 6], high strength at elevated temperatures and high work hardening rate [7]. This leads to a series of technical challenges for the manufacturers such as low productivity, short tool life [8, 9], vast use of cutting fluid and high machining cost.

Thermally assisted machining (TAM) methods have been proposed to enhance the machinability of these difficult-to-cut materials, in which a local heat source (e.g. laser beam, plasma beam [10]) is placed ahead of the cutting area to preheat the workpiece material locally and thereby reduce its strength during the machining process. With the rapid development of laser technology, laser assisted techniques now have many advantages over other pre-heating techniques, e.g. cost-effective and productive [11], while enabling higher energy intensities and making it easier to control the heating location and size [12] when compared with other methods (e.g. plasma, gas torch, electrical current heating). Laser assisted machining (LAM) has been reported to offer many advantages, such as reducing cutting forces [13, 14] and specific machining energy [15, 16], suppressing chatter [17], increasing material removal rates [18], extending tool life [19, 20], minimizing residual stresses[21, 22], generating crack-free machined surfaces [23], and diminishing environmental impact [24]. Accordingly, the LAM process is a very promising way to make these difficult-to-cut materials easier to machine [25].

Laser assisted turning (LAT) and laser assisted milling (LAMill) are the two most commonly used LAM processes. In LAT, the laser beam spot is placed ahead of the cutter to preheat the cutting volume locally [11] and the distance from the laser spot to the cutter is often fixed. LAMill is similar to LAT [26, 27] as the laser spot can be also projected on the cutting area [28] – this is the conventional way to use LAMill. Nevertheless, the fixed location of the laser spot relative to the cutting tool in the conventional LAMill process leads to a series of very challenging problems. Firstly, it is usually difficult to heat up the cutting volume in a homogeneous manner. Secondly, the maximum cutting width or depth in LAMill are constrained by the laser spot diameter, which becomes a very significant impediment when the width of cut is bigger than the laser spot size; hence, not surprisingly, LAMill has usually been demonstrated only for small cutting widths [29-32] comparable with the spot size of the laser. In addition, the optics system has to be changed to adapt to different cutting widths or depths, which is always time consuming.

More recently, Kang and Lee [33] heated up a workpiece surface in a region slightly wider than the spot diameter by applying a back and forth scanning method parallel to the feed direction. In their study, the location of the laser spot was fixed relative to the cutting tool and the workpiece was heated in two steps: first, they preheated the workpiece by one back and forth scan without cutting; then, when the laser spot had moved back to the cutting area together with the cutting tool, they performed conventional LAMill.

Nonetheless, very limited improvement can be achieved by this kind of scanning method in terms of covering large areas (i.e. width of cut for milling) and homogeneity of the HAZ.

To heat up an area far wider than the laser spot diameter effectively and with a homogeneous temperature distribution, a novel spatially and temporally (S&T) controlled laser heating method is proposed in this study. In our method, the laser spot oscillates along a specific trajectory to generate the targeted/predefined HAZ. Although a similar oscillatory heating method has been proposed by Bermingham et al [34], they neither gave any information on how to configure the laser scanning (e.g. laser power, scanning path and speed) nor presented results from this heating strategy.

In our study, we demonstrate the scientific derivation of the proper laser configuration by solving two heat conduction problems, i.e., the forward problem and the inverse problem. The forward problem is to determine the temperature distribution in the workpiece for a given laser beam configuration (i.e. laser power and motion), but the more important problem is the inverse problem, which is used to find the optimal configuration of the laser system (i.e. laser power, beam trajectory and scanning velocity) that results in a controlled 3D heat distribution within a zone of the workpiece that is to be cut, to enable the softening of the workpiece material and hence the improvement of its machinability.

The forward problem is the foundation for solving the inverse problem and its solution must be cheap to compute so that it can be used on real machine tools efficiently. Unlike the LAT process, in which the forward problem is relatively simple (as the laser spot has fixed position relative to the cutting edge) and has already been solved by both analytical [35] and numerical [36] methods, the forward problem in LAMill is more complex. Woo et al [37] and Van et al [38] derived a three-dimensional (3D) transient heat conduction model individually for a travelling heat source with uniform heat distribution for laser surface processing. However, the laser beam usually has a Gaussian distribution of heat flux [39]. Although Araya et al [40] developed a generic 3D transient heat conduction model of a moving Gaussian distribution plane heat source for a finite domain; it is too computationally expensive for our purposes. The finite element method (FEM) is another widely used technique [41, 42], but unfortunately is also too computationally intensive to be used to find the optimal solution.

To this end, the solution of the forward problem in LAMill enabling lightweight computation of transient 3D temperature distributions for an elliptic Gaussian distribution heat source moving with arbitrary trajectory, is still needed and is derived in this paper.

To the authors' best knowledge, there is no published research on the inverse problem for laser assisted machining. In this paper, the inverse thermal problem in LAMill was solved by two different methods: i) optimising the laser scanning speed and power for a predefined laser trajectory, i.e. the speed-optimised inverse problem; and ii) optimising the laser trajectory and power for a fixed laser scanning speed, i.e. the path-optimised inverse problem. Modelling results indicated that both methods are effective, but only the path-optimised trajectory was verified by experiment due to limitations of the laser scanning system. The solution of the inverse problem in LAMill , with high widths of cut compared with laser spot size, has been extensively validated by evaluating the surface and bulk temperatures in the HAZ as well as by

cutting experiments (with evidence of significant decrease of cutting forces) and metallurgical analysis of cut surfaces.

2 Novel spatial and temporal controlled heating method for laser assisted milling (LAMill)

In conventional laser assisted milling, the position of the laser spot relative to the cutting tool is fixed, which leads to significant non-uniformity of temperature in the HAZ, limiting its industrial application to widths of cut comparable to the laser spot diameters. It is therefore no surprise that LAMill is mainly reported for small diameter cutting tools.

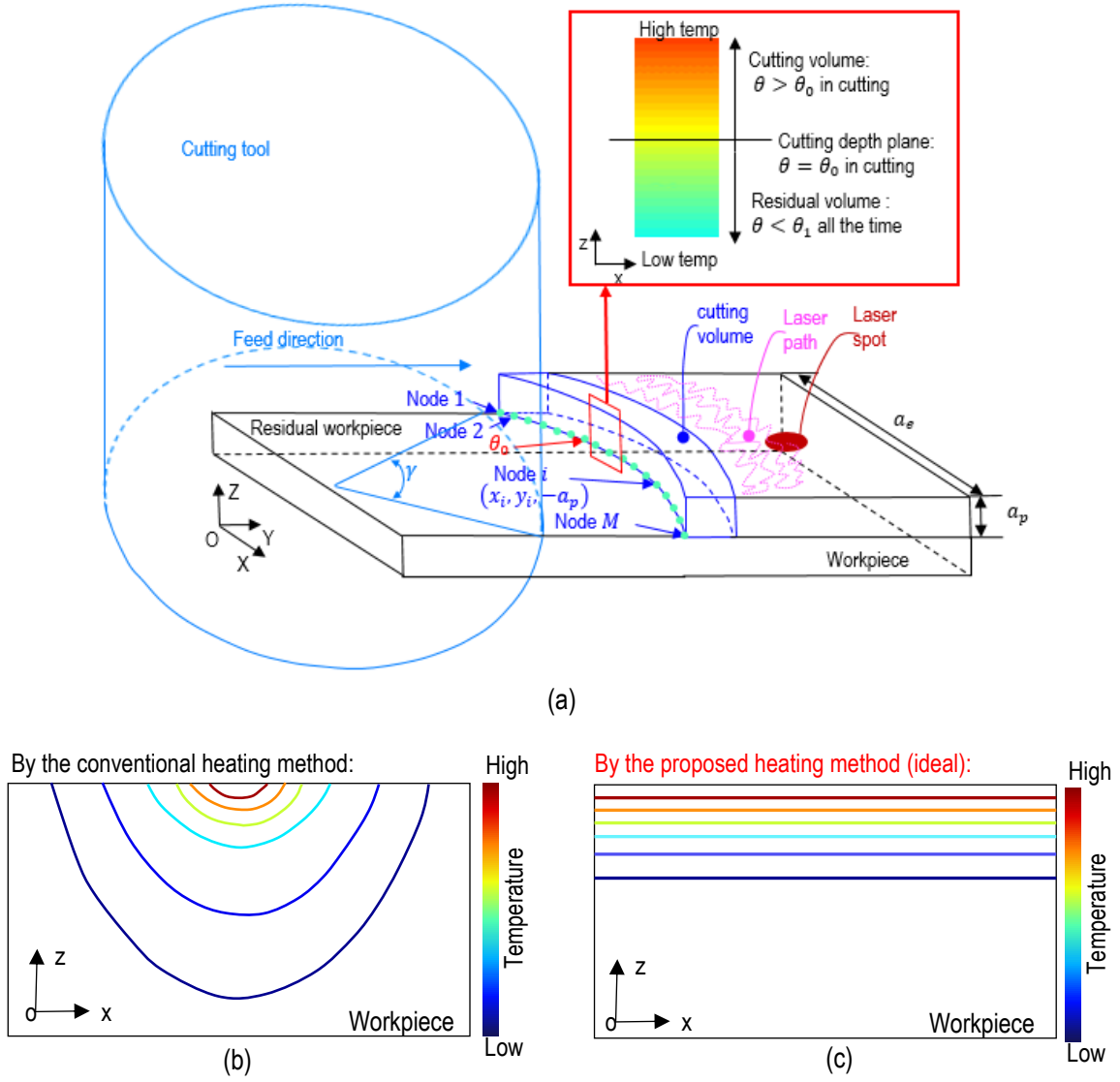

Fig. 1 S&T controlled laser heating method in LAMill: (a)schematic diagram on the S&T controlled laser heating method and ideal temperature distribution, and theoretical temperature distribution improvement on the cutting cross-section from (b) the conventional laser heating method - fixed spot position and (c) the proposed S&T controlled laser heating method – inversely optimised laser scanning trajectory

In the method proposed in our work (as shown in Fig. 1(a)), the laser spot scans ahead of the cutter along the cutting direction (perpendicular to the feed direction), which allows an area far wider than the spot size to be heated to an almost homogeneous temperature by optimising the laser scanning trajectory for given cutting parameters and material properties; note that the path of the laser scanning is not predefined and it can take any trajectory which is governed by the solution of the inverse problem (to be presented later). Fig. 1 (b) and (c) illustrates the theoretical temperature distribution for the conventional (i.e. fixed position of the laser spot) and proposed (i.e. optimised laser path) methods for LAMill. Although a similar approach has been proposed in [34], the scientific derivation of the real problem is still missing, i.e. optimise the laser parameters and path of the laser ahead of the cutting tool to ensure that a specified temperature distribution is achieved when the edges of the milling cutter engage the workpiece. This is the inverse problem, and in the following we solve it for the first time and clarify, in a scientific way, how the process should be controlled to achieve the required performance regardless of specifics of the setup.

3 Modelling of laser heat placement

3.1 Forward problem: temperature distribution by freeform laser trajectory

The forward heat conduction problem is to calculate the temperature distribution in the workpiece for an arbitrarily prescribed laser trajectory, which is the foundation of laser heat placement control. We assume that the workpiece bulk is initially in thermal equilibrium with ambient, treat the bulk volume as semi-infinite in the z direction, and neglect heat losses from the upper surface because they are small compared to the laser heat absorbed by the workpiece (i.e. an diabatic upper surface boundary). The governing equation of three-dimensional transient heat conduction [43] is

$$\frac{\partial^2\theta}{\partial x^2}+\frac{\partial^2\theta}{\partial y^2}+\frac{\partial^2\theta}{\partial z^2}+\frac{1}{k}q'''(x,y,z,t)=\frac{1}{\alpha}\frac{\partial\theta}{\partial t} \tag{1}$$

where $\theta=\theta(x,y,z,t)$ is the temperature at time t, (x,y,z) are Cartesian coordinates fixed in the workpiece (as shown in Fig. 1(a)), $q'''(x,y,z,t)$ is the Gaussian laser spot heat source (shown in Eq. (A2)), $\alpha=k/\rho c$ is the thermal diffusivity in m^2/s, k, ρ, c are thermal conductivity (W/(m K)), density (kg/m^3) and heat capacity (J/(kg K)) of the workpiece material, respectively. Eq. (1) was solved by the Green's function method (a more detailed derivation is given in the Appendix) and the solution is

$$\begin{aligned}\theta(x,y,z,t)=\frac{2\alpha}{k}q_0\int_{\tau=0}^{t}&\frac{1}{\left(4\pi\alpha(t-\tau)\right)^{\frac{3}{2}}}\frac{4\pi}{\sqrt{\frac{4}{r_{bx}^2}+\frac{1}{\alpha(t-\tau)}}\sqrt{\frac{4}{r_{by}^2}+\frac{1}{\alpha(t-\tau)}}}\\&\times\exp\left(-\frac{\left(x-x_b(\tau)\right)^2}{r_{bx}^2+4\alpha(t-\tau)}\right)\times\exp\left(-\frac{\left(y-y_b(\tau)\right)^2}{r_{by}^2+4\alpha(t-\tau)}\right)\\&\times\exp\left(-\frac{z^2}{4\alpha(t-\tau)}\right)d\tau\end{aligned} \tag{2}$$

where $q_0 = \eta P/(\pi r_{bx} r_{by})$, in which η is the laser heat absorption ratio by the workpiece material and P is the laser power, r_{bx} and r_{by} are the semi-length of the major axis and the minor axis of the elliptic laser spot respectively, $(x_b(t), y_b(t))$ is the transient position of the laser spot. We evaluated the integral in (2) using Gauss-Legendre quadrature. Because there is no limitation on the laser beam path, (2) is suitable for arbitrary laser beam trajectories.

3.2 Inverse problem: method for controlling laser heat placement

The inverse problem is to find the optimal laser configuration (laser power, laser speed and location) for the target temperature distribution (which is related to the need to soften the workpiece material when the cutting takes place in LAMill). Regarding the LAMill process, the cutting volume (as shown in Fig. 1 (a)) should be heated up to a specified temperature θ_0 which depends on the material properties so that the cutting volume can be effectively softened. Additionally, the temperature distribution needs to be as homogeneous as possible along the cutting cross-section to make the cutting process stable and obtain a uniform machined surface.

The inverse problem can be transformed into a continuous optimization problem, in which the appropriateness of the current laser configuration is expressed by the cost function

$$C = \frac{1}{M}\sum_{i=1}^{M}\left(\theta_{x_i,y_i,-a_p} - \theta_0\right)^2, \tag{3}$$

Which is to be minimized, with θ_0 the target temperature, $\theta_{x_i,y_i,-a_p}$ the temperature caused by laser heating at the position (x_i, y_i) at the depth of cut and M is the number of mesh nodes (as shown in Fig. 1 (a)) for the evaluation of the temperature distribution.

To make the laser scanning physical achievable and avoid overheating of the workpiece, the following constraints should be satisfied:

- *Avoid overheating of the residual workpiece material that would affect its microstructure*. As shown in Fig. 1 (a), this is the main constraint for the inverse problem which requires that the HAZ that can cause phase change, should be shallower than the depth of cut, so that

  $$\theta(x, y, -a_p, t) < \theta_1 \tag{4}$$

  in which θ_1 is the critical temperature for the material to change the metallic crystal by laser heating.

- *Laser power should be within the power supply range of the laser source*. This can be expressed as

  $$P_{min} \le P \le P_{max} \tag{5}$$

  where P is the laser power, and P_{min} and P_{max} are the lower and upper bounds on the power of the laser system.

- *Laser speed cannot exceed an upper bound allowed by the laser scanner*. This can be formulated as

$$v_b \leq v_{b-max} \tag{6}$$

with v_b and v_{b-max} the transient speed of the laser spot and the max scanning speed that can be achieved by the laser system, respectively, and $v_b(t) = \sqrt{\left(\frac{dx_b}{dt}\right)^2 + \left(\frac{dy_b}{dt}\right)^2}$.

- *Laser scanning acceleration should be physically achievable by the laser system*. This gives

$$a_b \leq a_{b-max} \tag{7}$$

where a_b and a_{b-max} are the laser acceleration and corresponding max value respectively.

From simulations, we found that for rapid, periodic scans of the laser beam, the temperature distribution becomes quasi-static after several cycles (for example, 20 scans in our simulation). By using a periodic laser trajectory we significantly reduced the computation time because only one period needs to be optimized.

The laser beam configuration is defined by the fixed power and position as a function of time, namely (P, x_{bj}, y_{bj}, t_j), where j is the index of the discrete laser trajectory, and can be optimised in two ways:

- *Laser speed optimization for a fixed scanning path.* In this case, the laser scanning path (X_{bj}, Y_{bj}) was predefined and t_j which is equivalent to laser speed was optimised.
- *Laser scanning path optimization for fixed laser speed.* In this case, (X_{bj}, Y_{bj}) was optimised while t_j was fixed as a linearly increasing function of its index j in order to obtain the required fixed period, T_b (see below).

We used a standard interior point algorithm (fmincon in MATLAB) to solve the optimization problem. In the following, we take the high feed milling process as an example to demonstrate the solution procedure for the inverse problem.

3.2.1 Inverse problem: by laser scanning speed optimization

In this case, the laser path is defined before optimising the laser speed. The laser path was defined by the parametric equation

$$\begin{cases} x_b = x_{b0} + R_b \sin(\phi_b) \\ y_b = y_{b0} + f_y t + R_b \cos(\phi_b) \end{cases} \tag{8}$$

which consists of a series of smooth arcs with a similar shape to the cutting area of the milling tool, where (x_b, y_b) is the position of the laser beam, (x_{b0}, y_{b0}) is the initial scanning centre of the laser spot, f_y is the feed rate of the cutting process, $\phi_b = -\gamma\cos(2\pi t/T_b)$, T_b is the period of the laser scanning, γ is the central angle of the cutting area (shown in Fig. 1 (a)), R_b is the effective cutting

radius. T_b is determined by the minimum number of overlaps between the laser traces. For example, if the minimum overlap amount is m, then we will have $T_b \leq d/(f_y m)$, where d is the laser spot size along feed direction. Because Eq. (8) has infinite order continuous derivatives, the laser path is very smooth everywhere (as illustrated in Fig. 2). In addition, there are more points at the corners of the laser path (as shown in Fig. 2 (b) and (c)) when we discretise the time t in Eq. (8) into a linearly increasing series of its index, which is good for describing the laser path precisely.

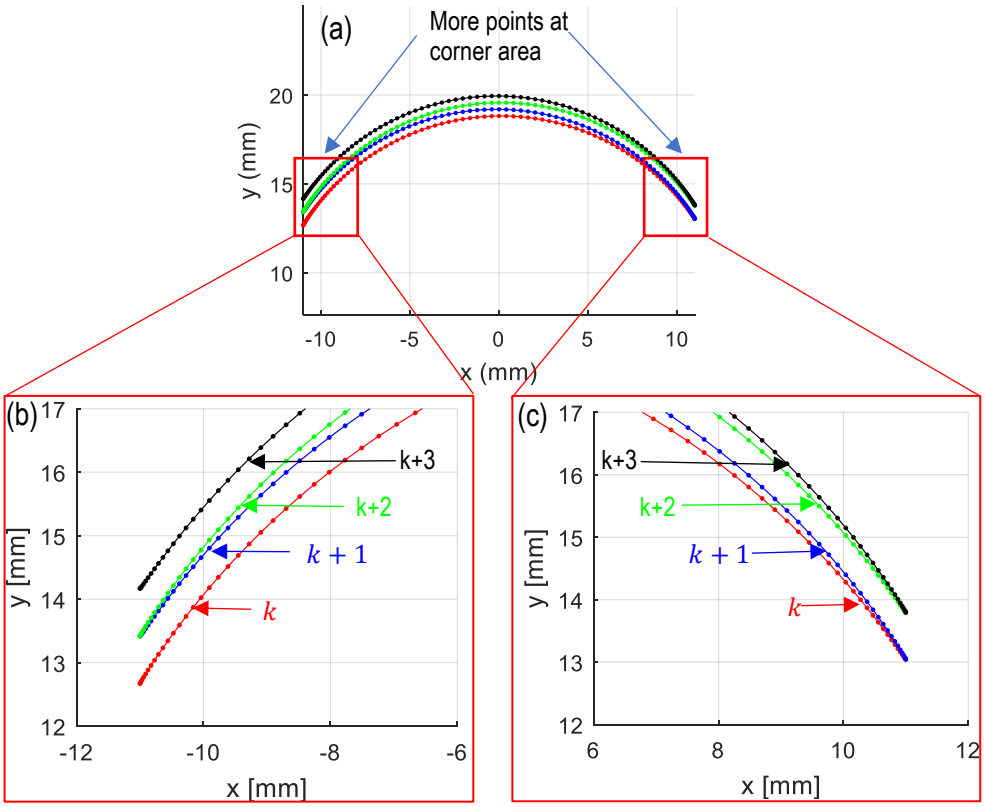

Fig. 2 Inverse problem with predefined laser trajectory for speed optimization: laser scanning path (a) and enlarged view at left corner (b) and right corner (c) area for k^{th} to $(k+3)^{th}$ scanning

We must now solve an optimization problem which can be summarized as minimizing the deviation from the target temperature distribution (shown as Eq. (3)) by optimising the laser power P and the laser scanning speed at each point of the predefined laser path (defined by Eq.(8)) subject to the constraints Eq. (4) to (7).

Since the laser configuration is defined by (P, x_{bj}, y_{bj}, t_j), the series t_j specifies the laser speed as long as the laser scanning path is predefined. Thus the control parameters are the laser power P and time series t_j in the inverse problem by laser scanning speed optimization.

In order to give a representation of our simulations, we present a set of results from modelling using the parameters: cutting width=19mm, cutting depth=0.26mm, feed rate=948mm/min (0.5mm/tooth) and laser beam diameter=3mm. After optimization, the new time series and laser scanning speed were compared in Fig. 3 while the initial and optimised temperature distribution were shown in Fig. 4 and Fig. 5, respectively. The optimised HAZ has a similar shape to the cutting area (Fig. 5 (a) and (b)) and

dramatically, the temperature distribution becomes much more homogeneous along the cutting cross section (Fig. 5 (c)).

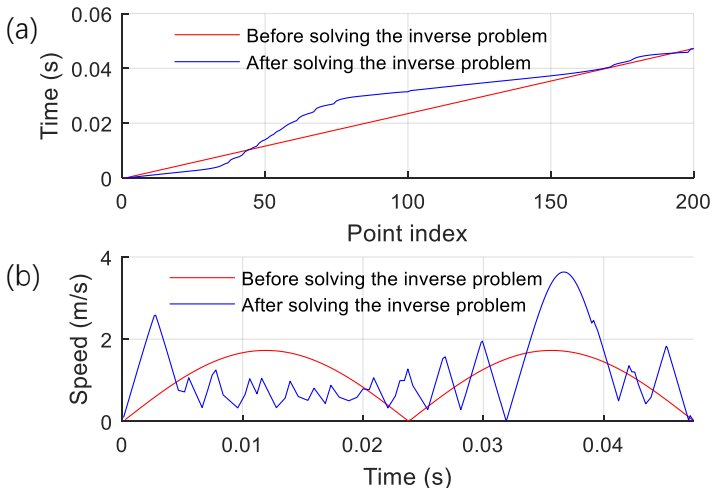

Fig. 3 Comparison of laser scanning trajectories before and after solving the inverse problem by speed optimization: time series t_j in laser scanning configuration (P, x_{bj}, y_{bj}, t_j) (a) and laser scanning speed in one scanning cycle (b)

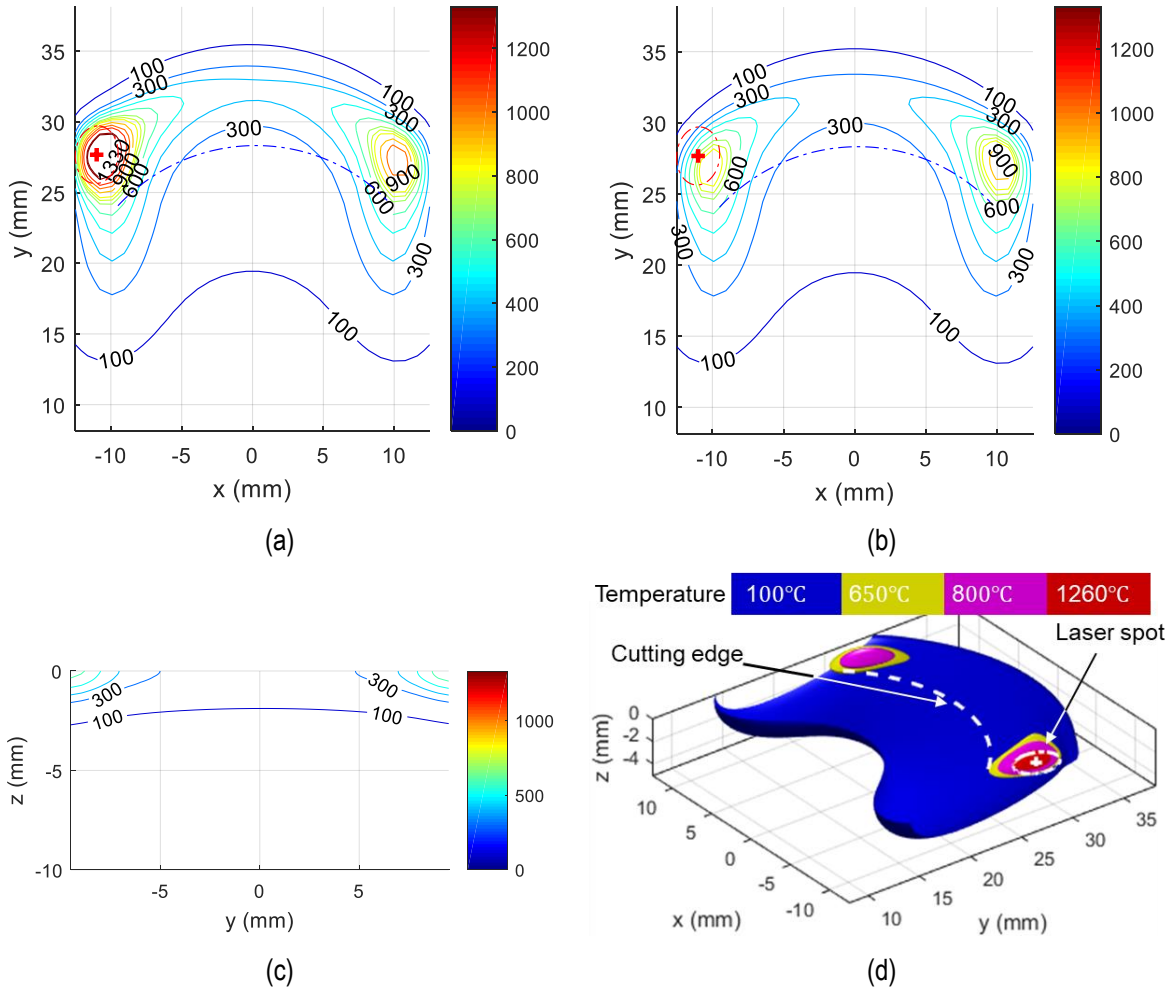

Fig. 4 Predicted temperature distribution for the initially chosen laser trajectory: on the top surface (a), on the depth of cut plane (b), along the cutting cross section(c) and the 3D view (d). Parameters used were: cutting width=19mm, cutting depth=0.26mm, feed rate=948mm/min (0.5mm/tooth) and laser beam diameter=3mm.

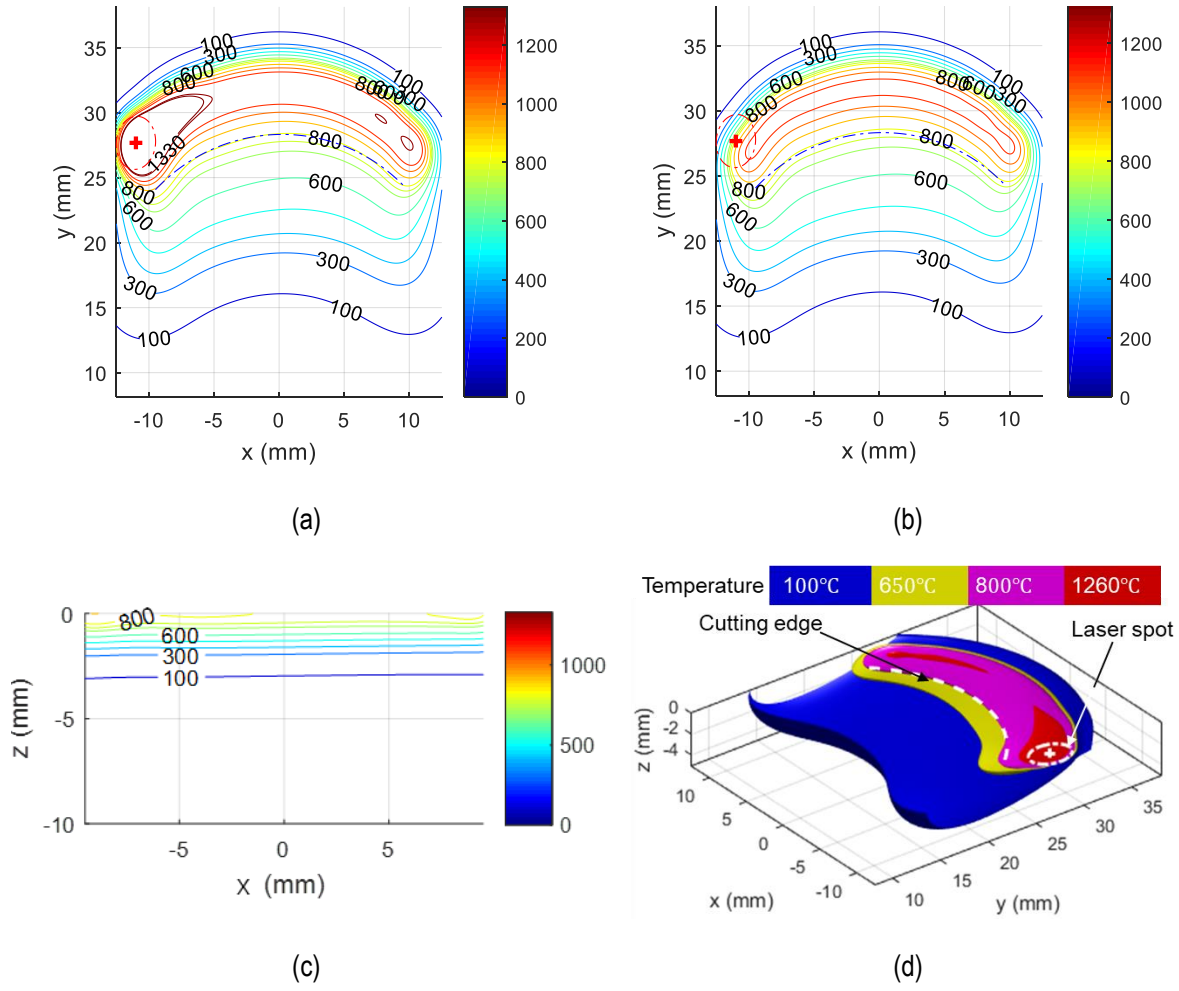

Fig. 5 Predicted temperature distribution for the speed-optimised laser trajectory: on the top surface (a), on the depth of cut plane (b), along the cutting cross section(c) and the 3D view (d). Parameters used were: cutting width=19mm, cutting depth=0.26mm, feed rate=948mm/min (0.5mm/tooth) and laser beam diameter=3mm.

3.2.2 Inverse problem: by laser scanning path optimization

The second way to solve the inverse problem is to optimize the laser path while limiting the variation of the laser scanning speed. In this case, the laser trajectory (x_{bj}, y_{bj}) and laser power were the control parameters to be optimised while the time series t_j was fixed as an independent variable. To limit the variations of the laser scanning speed, we imposed the constraint

$$\max\left(\left|\frac{v_b - \overline{v_b}}{\overline{v_b}}\right|\right) \leq 0.05 \tag{9}$$

where v_b is the transient laser scanning speed and $\overline{v_b}$ is the average speed during one scanning cycle.

Besides the constraints described by Eq. (4) ~ Eq. (7) and Eq. (9), the safe distance between the laser spot to the cutter (as shown in Fig. 6) also has to be considered to avoid damage of the tool by the laser beam. This distance can be obtained from Eq. (10) and this safe distance constraint can be described by

$$d_{bt} = \min\left(\sqrt{\left(x_{bp} - x_{tc}\right)^2 + \left(y_{bp} - y_{tc}\right)^2}\right) - R_t \tag{10}$$

$$d_{bt} \geq d_{bt-min} \tag{11}$$

where d_{bt} is the minimum distance from one point at the cutting tool border to another point at the laser beam edging, (x_{bp}, y_{bp}) is the point at the edge of the laser spot and (x_{tc}, y_{tc}) is the cutting tool center (Fig. 6), R_t is the radius of the cutting tool, d_{bt-min} is the required safe distance.

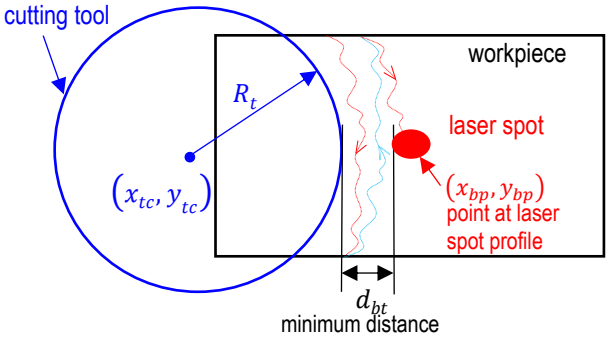

Fig. 6 Illustration of the safe distance between laser spot and cutting tool from top view during laser scanning

Starting from the trajectory defined in Fig. 2, the path-optimised laser trajectory is shown in Fig. 7, in which the laser scanning path becomes a freeform curve but the laser speed is constant. The corresponding temperature distribution was presented in Fig. 8, where the temperature distribution in the cutting volume is almost homogeneous.

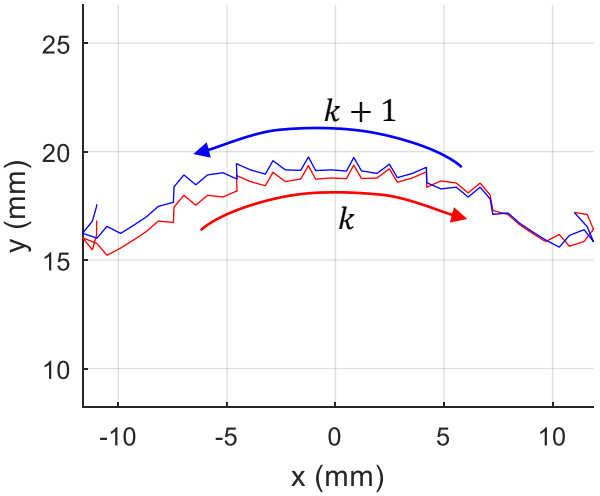

Fig. 7 Laser scanning path of one scanning cycle from the path-optimised inverse problem, the red line showed the forward scanning path while the blue one is the backward path

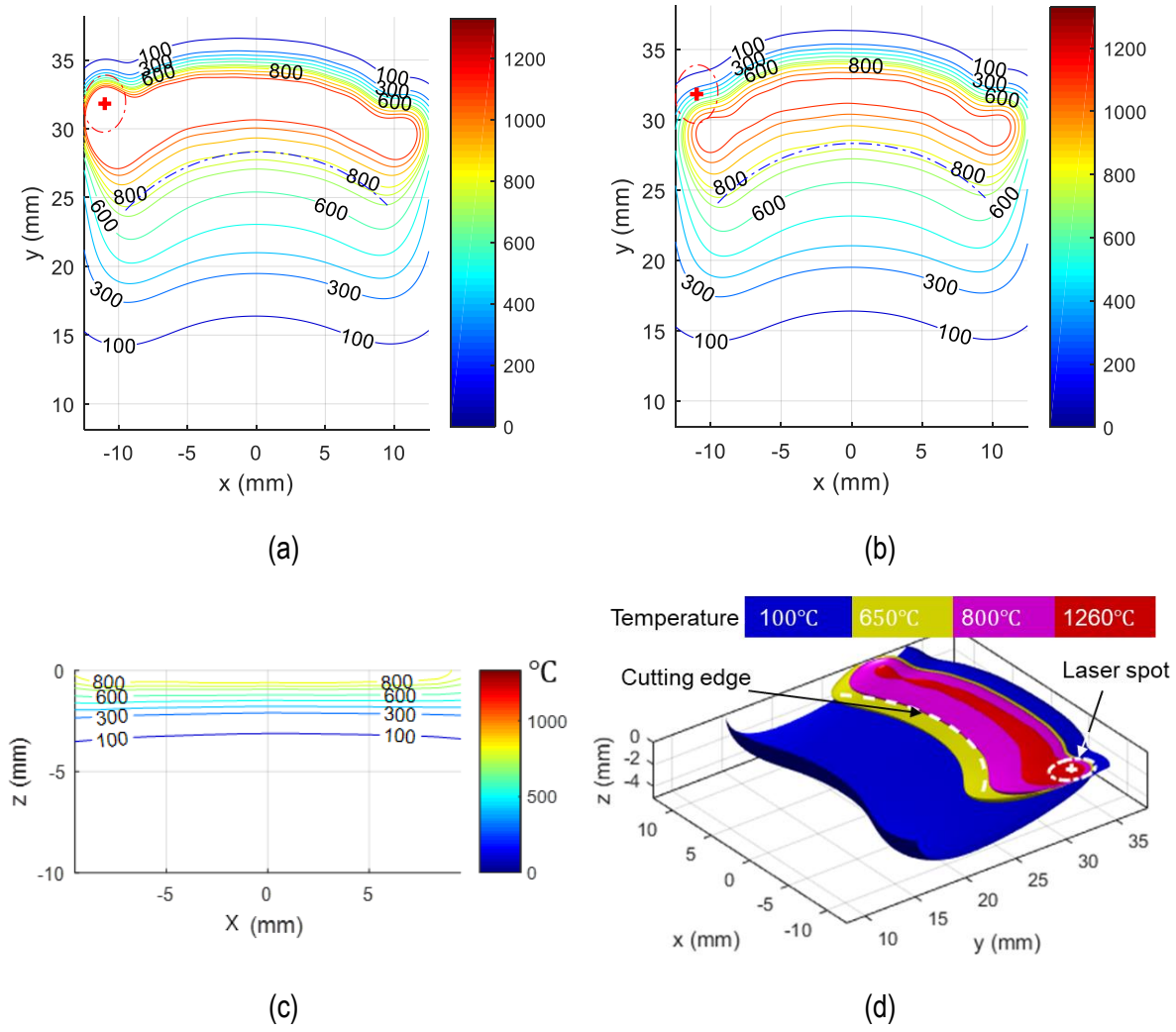

Fig. 8 Temperature distribution for the path-optimised laser trajectory: on the top surface (a), on the depth of cut plane (b), along the cutting cross section(c) and the 3D view (d). Parameters used were: cutting width=19mm, cutting depth=0.26mm, feed rate=948mm/min (0.5mm/tooth) and laser beam diameter=3mm.

4 Experimental validation and discussion

4.1 Experimental setups

A series of experimental tests was conducted on the platform shown in Fig. 9, where a 5-axis milling machine tool integrating a 10kW diode laser system (LDF mobile laser power made by LASERLINE Inc., laser spot diameter is 3mm) was used. The 2-axis laser beam deflection unit SUPERSCAN-LD-30 which was mounted on the spindle head was employed to control the laser location. The surface temperature was measured by FLIR A325 infrared (IR) camera (IR resolution 320×240 pixels, image frequency 60Hz, spectral range 7.5~13μm and measure temperature range -20~2000°C) beside the workpiece while the temperature inside the workpiece was recorded by a K-type thermocouple array (sheath diameter 0.25mm, respond time ca. 15μs and measuring range -270~1372°C) embedded into the workpiece. Considering the drilling depth error of holes for thermocouples mounting, the depth of each hole was carefully calibrated before fixing the thermocouples in. Thermocouple signals were logged by an NI-1102B unit, which has a maximum multiplexing sampling rate 333kS/s with 0.012% error. Square bar

samples of precipitation hardened Inconel 718, of which the relevant physical and thermal properties are shown in Table 1, were cut by the high feed milling tool (32 mm R217.21-3232.0-LP06.4A tool shank with four LPHT060310TR-M06 MS2050 type inserts) made by SECO TOOLS. The cutting forces were captured by an ATI dynamometer (model Omega191 IP65/IP68) with 36 kHz sampling rate.

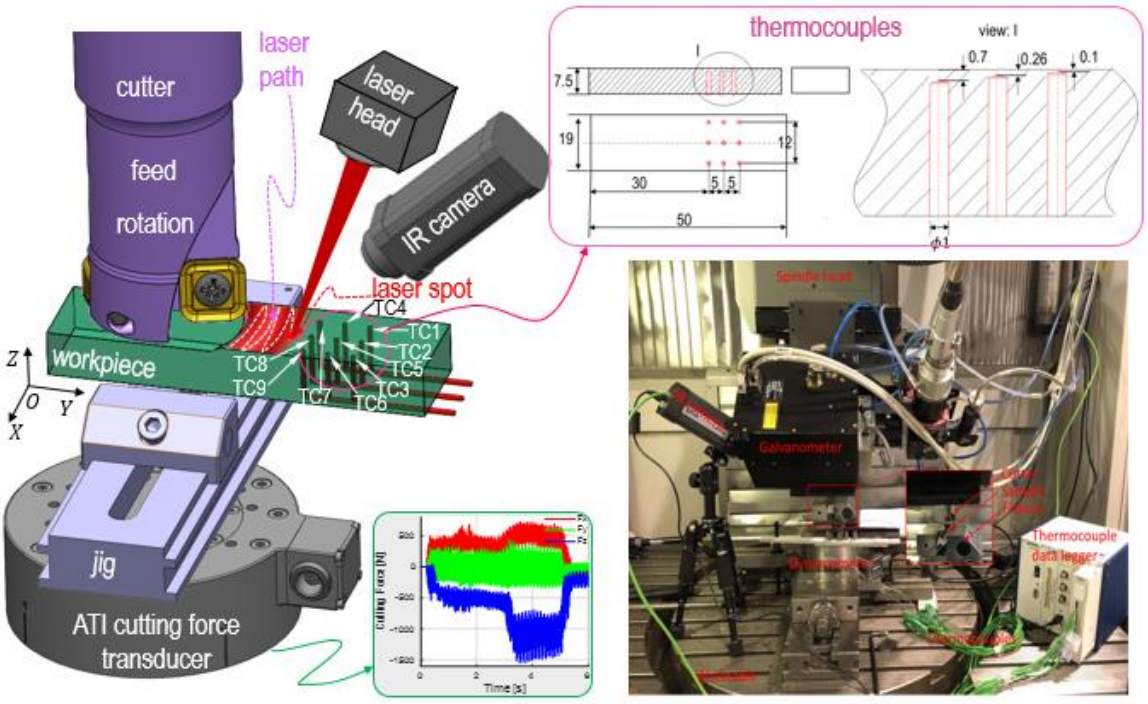

Fig. 9 Experimental set-up for the LAMill, in which the temperature on the top surface was captured by thermal camera while inside was logged by thermocouple array, and cutting forces was monitored by ATI multi-channel dynamometer

Table 1 Relevant physical and thermal properties of Inconel 718[16]

Property	Value
Density	8193~8220 kg/m^3
Melting range	1260~1336℃
Specific heat capacity	1e3(0.0002*T+0.4217) J/(kg K)
Thermal conductivity	0.015*T+11.002 W/(m K)

4.2 Forward problem verification

Verification of the forward problem is to test the prediction error of the forward heat conduction model for different laser trajectories. To achieve this, two laser scanning tests were conducted, i.e. linear and cosine trajectories during which the temperature on the top surface was measured by the IR camera.

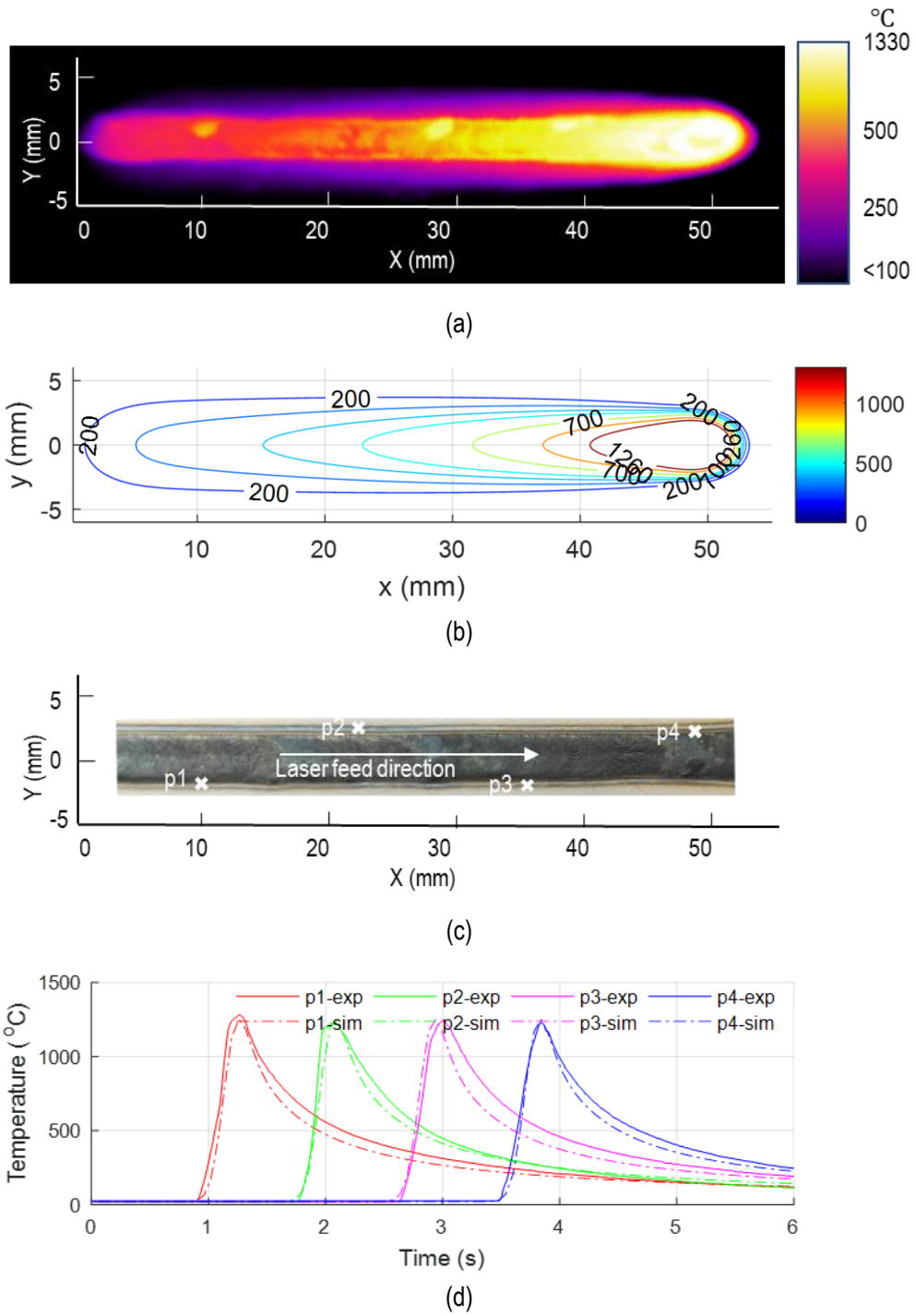

Fig. 10 Experiment results on direct problem for linear laser path scanning: measured (a) and simulated (b) temperature on the top surface, photo of the sample surface (c) and comparison between experimental (exp) and simulated (sim) temperatures at four selected points (P1~P4) (d)

The linear moving laser beam is the simplest case of a moving heat source problem, so this test can test the basic ability of the forward heat conduction model. The laser power and laser feed speed were 2000W and 900mm/min respectively in the test. The laser heat was concentrated around the laser spot which left a “comet tail” like heat distribution (as Fig. 10 (a)) as well as a melted ribbon area (as Fig. 10 (c)). The shape of the simulated temperature distribution shown as Fig. 10 (b) matched well with the thermographic image, and to further estimate the error range, temperature change at four points (shown in Fig. 10 (c))

were compared in Fig. 10 (d). Results showed that the simulated temperature change is very close to the measured and the average error range of the peak temperature is within 15%. However, the simulated temperature cools down faster than the measured temperature (as shown in Fig. 10 (d)). This is because the workpiece was assumed to be semi-infinite thus the laser heat was dissipated to the infinite volume. However, the real case is that the laser heat is accumulated in the workpiece and then dissipated to the ambient environment. The thermal conductivity from the workpiece to ambient can be approximated as the conductivity of air (0.0262 W/(m K) which is far smaller than the internal heat conductivity of the workpiece (11.302 W/(m K)) thus the real cooling-down speed is slower than the simulated.

A cosine wave trajectory is the simplest possible periodic trajectory, which can also capture the dynamics of the laser galvanometer. Parameters of the cosine wave trajectory are amplitude=15mm, period=1.2s and wavelength=24mm and the laser power used was 2000W. Similar to the linear scanning case, the simulated and measured temperature distribution were compared in Fig. 11. The results showed that the temperature distribution matched well between simulation and measurement and the errors of the peak temperature of the selected points is within 10%. Again, the simulated temperature decreases a little faster than actual for the reasons noted above. For example, cooling time from the peak temperature to 500°C in simulation is 0.1968s while this value was measured as 0.2343s.

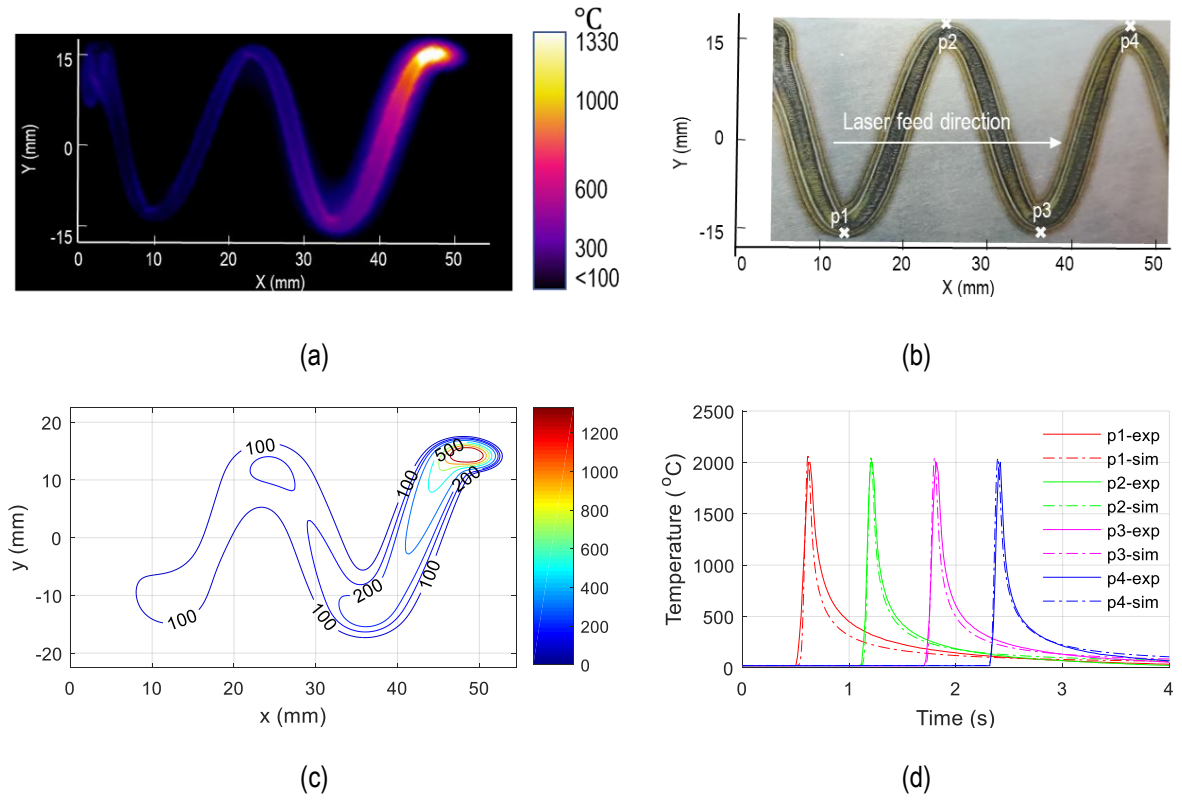

Fig. 11 Experiment and simulation results of cosine wave scanning: measured (a) and simulated (c) temperature on the top surface, photo of the sample surface (b) and comparison between experimental (exp) and simulated (sim) temperatures at four selected points (P1~P4) (d)

The accuracy of the forward heat diffusion model is within 15% for both linear and cosine wave scanning tests, and better for the cosine wave scanning. This suggests that the forward heat conduction model

can predict the temperature distribution for both simple and complex laser scanning trajectories with similar accuracy, which is a good foundation for the inverse problem.

4.3 Inverse problem verification

The proposed S&T controlled laser-heating method was verified by laser scanning tests. Both the path-optimised and speed-optimised trajectories from the inverse thermal problem were scanned while the upper surface temperature distribution was captured by the thermal camera and the inner workpiece temperature by thermocouple arrays.

To demonstrate the verification of the inverse problem, we take the high feed milling process of Inconel 718 as an example (cutting width, depth and feed rate are 19mm, 0.26mm and 0.5mm/tooth respectively with the laser beam diameter 3mm). The target temperature θ_0 in Eq. (3) was set as $800℃$ according to the high-temperature mechanical properties of Inconel 718 [44] when the material softening effect occurs, while the overheating temperature θ_1 in Eq. (4) was selected as its melting point of 1260°C [45].

Trajectories from the inverse problem by both methods, i.e. speed-optimization and path optimization, have been tested by scanning the laser beam using the galvanometric device. However, it was found that the laser galvanometer could not cope with the sudden changes in velocity that are required by the speed-optimised trajectory. The laser beam was stuck at some discrete positions as illustrated in Fig. 12(a) and these stagnations can also be seen from the sample surface presented in Fig. 12(c). To this end, the temperature distribution by the speed-optimised trajectory was found inappropriate for our hardware, i.e. the galvanometric scanner, because it doesn't have the speed control mode and the speed was input manually point by point leading to the discontinuous error.

For the path-optimised trajectory, the temperature distribution shape on the top surface (shown in Fig. 12(b)) was very close to the simulation result (shown in Fig. 8). To evaluate the error range of the inverse problem quantitatively, the temperature inside the sample was captured by thermocouple arrays (as shown in Fig. 9) and the results of TC1-8 were shown in Fig. 13 (a). The measurement error of these thermocouples is found about $\pm 2.69\%$ which stem from two factors: the accuracy of the thermocouples which is calibrated as $\pm 0.75\%$, and the assembling error of thermocouples which is around $\pm 1.94\%$ by calculating the temperature with the measurement error ($\pm 0.02\mathrm{mm}$) of the hole depth. And as a comparison, the expected temperature was also presented in Fig. 13 (b), from which the temperature change inside the sample during scanning the trajectory form the inverse problem matched well with its expectation. To further demonstrate this, the peak temperature during the scanning was compared in Fig. 14. The results showed that the maximum temperature deviation between measured and simulated distributions is within 10%.

The sample surface after scanning was shown in Fig. 12(d), from which the upper surface of the sample was dioxide homogeneously, particularly in the centre area while the edge area (about 3mm at each side) was a bit worse. This is because the sample was assumed as semi-infinite during modelling to simplify the problem, and this assumption led to the actual temperature at the edge area to be higher than that

from simulations. This can be overcome by employing the forward conduction solutions for a finite bulk if necessary; however, this will inevitably increase the computation cost.

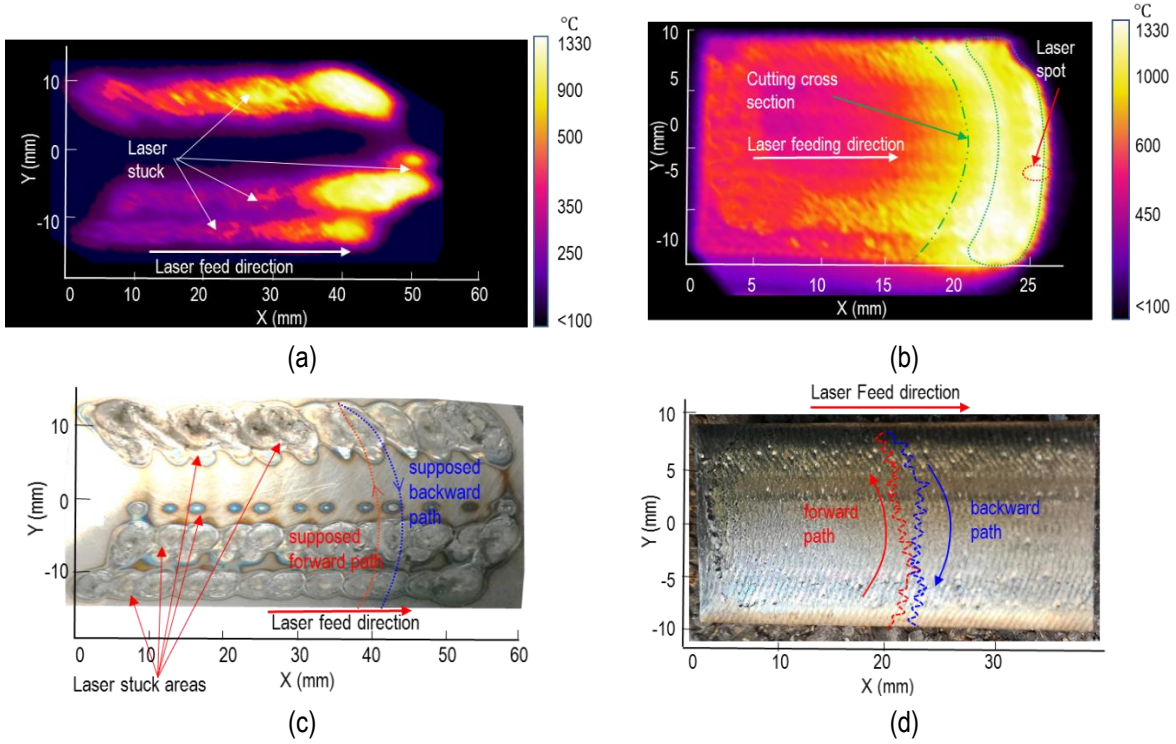

Fig. 12 Temperature distributions when scanning the two trajectories from the inverse problem (without machining): temperature distribution when scanning with the speed-optimised trajectory (a) and path-optimised trajectory (b) as well as workpiece surface after scanned by speed-optimised trajectory (c) and path-optimised trajectory (d). Note that the speed-optimised trajectory, (a) and (c) could not be implemented on the machine due to the limitations of the galvanometric scanner.

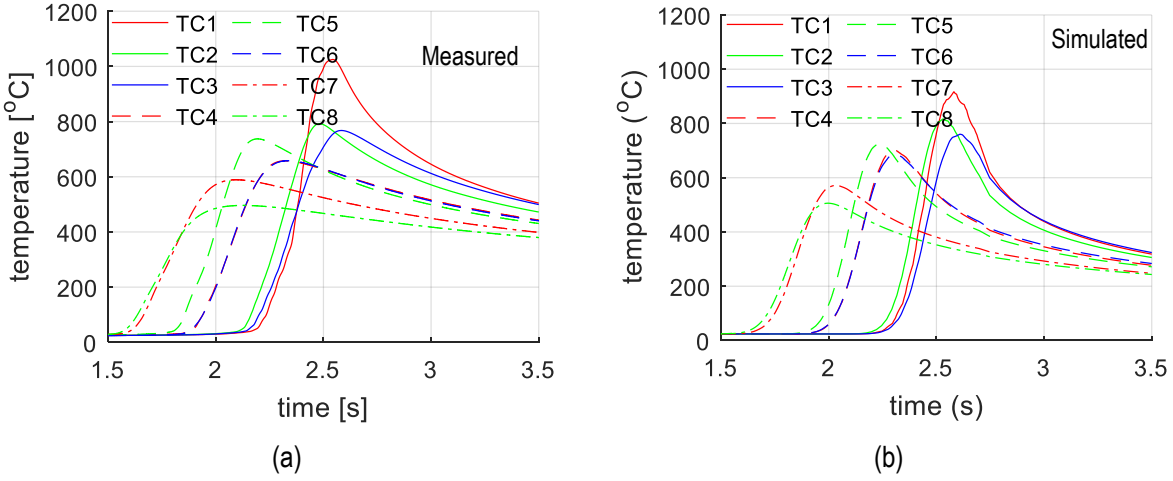

Fig. 13 Temperature change inside the sample during scanning of path-optimised laser trajectory: captured by thermocouple arrays (TC1~TC9 were shown in Fig. 9) (a) and comparison with simulation results (b)

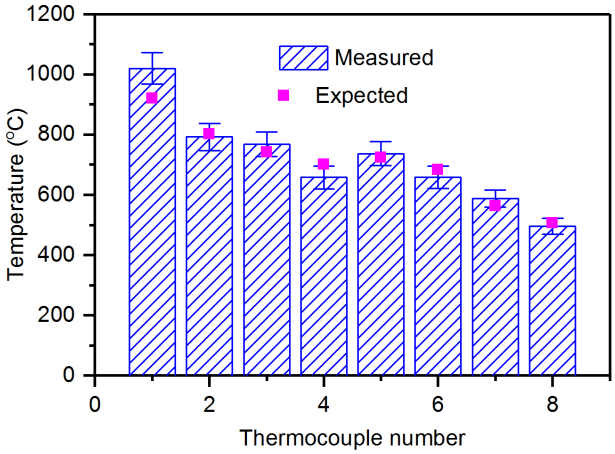

Fig. 14 Comparison of the peak temperature during scanning the laser trajectory from the inverse problem with its expectation

4.4 Laser assisted milling tests

Machining tests were also carried out to demonstrate the effectiveness of the proposed S&T controlled laser-heating method and cutting parameters were shown in Table 2. The reduction of the principal cutting force, which is the axial thrust force F_z along the cutting tool for high feed milling, due to laser heating was selected as the key performance indicator (KPI) to evaluate the benefits obtained by laser heating. Considering the impacts of tool wear condition on the cutting force, laser assisted milling and the benchmark conventional dry milling were conducted sequentially in one single milling pass and the tool wear condition was checked after each cutting pass to make sure that the tool presented very limited wear. Meanwhile, surface roughness and subsurface microstructure were analysed to make sure that the machined workpiece quality was not deteriorated by using LAMill process.

Table 2 Machining parameters employed to demonstrate LAMill process

Cutting width a_e [mm]	Cutting depth a_p [mm]	Feed rate f_r [mm/tooth]	Cutting speed v [m/min]
19	0.26	0.5	41

Laser scanning speed and laser power were 1.5m/s and 4800W respectively in the path-optimised LAMill. The measured and simulated temperature within the workpiece are presented in Fig. 15 (a) and (b) respectively while the deviation between the simulated and measured peak temperature are shown in Fig. 15 (c). From the results, the deviation is at the same level (lower than 10%) with the laser scanning case shown in Fig. 13 though the machining heat was ignored. This is because the machining generated heat, which can be estimated by cutting force and speed, is relatively low (ca. 274W in this case) due to material softening by laser and only a small portion (e.g. 17% [46]) was conducted to the workpiece. In addition, the additional heat losses on the upper surface due to the air turbulence induced by cutting tool might also neutralize the contribution of machining generated heat. These heat losses (Φ) can be estimated as 163.9W by the product ($\Phi = A\Delta h\Delta\theta$) of projection area of the HAZ on the upper surface (A) with the increase of the heat convection coefficient compared with laser scanning case (Δh) and the temperature difference of the upper surface to the ambient environment ($\Delta\theta$). To this end, both the heat

convection on the upper surface and the cutting heat effect were ignored in the modelling of the forward problem.

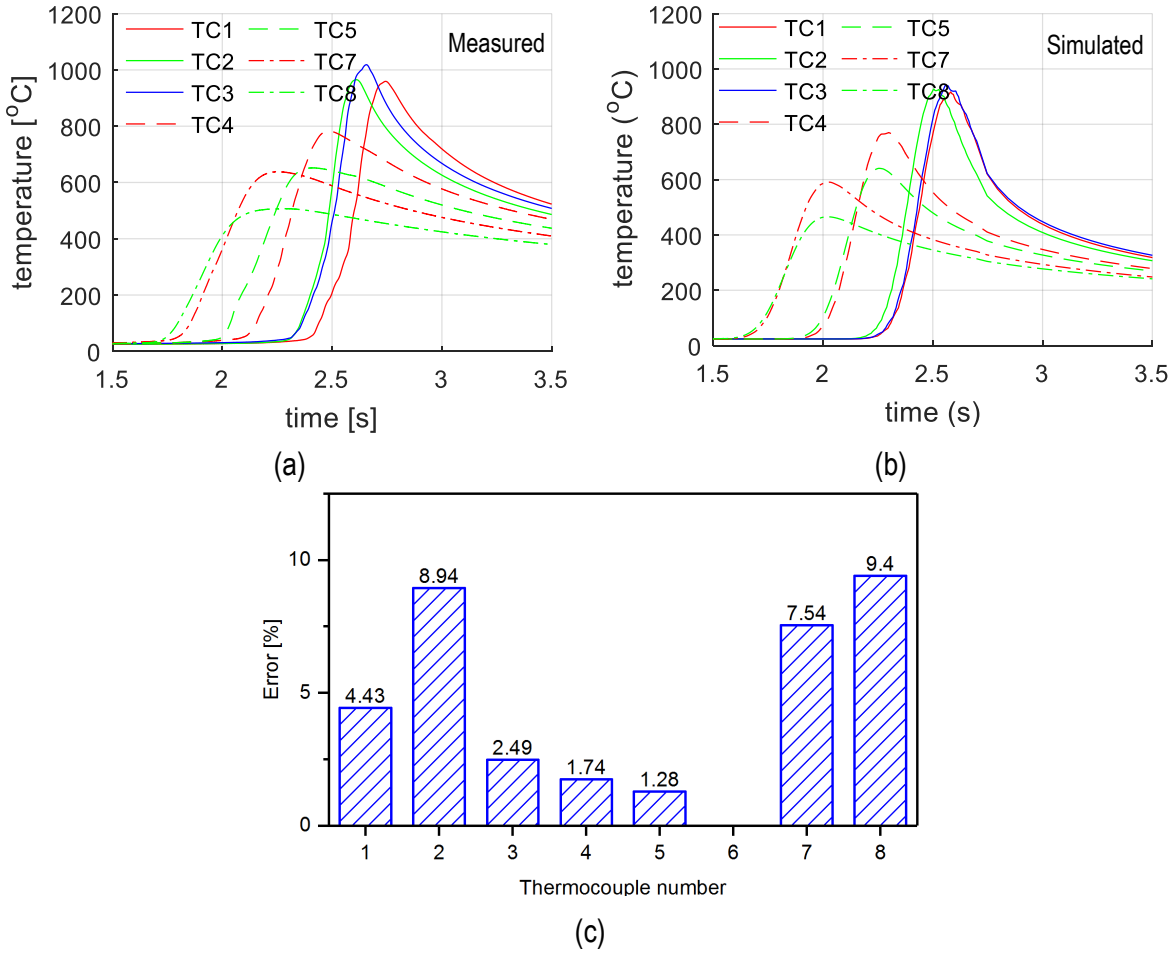

Fig. 15 Temperature change inside the sample LAMill of path-optimised laser trajectory: captured by thermocouple arrays (TC1~TC9 were shown in Fig. 9) (a) and comparison with simulation results (b) and the errors of the peak temperature (c)

Cutting forces during the test are presented in Fig. 16, where the first half was for LAMill and the second half was for dry milling. The mean and peak value of the cutting force during the stable cutting period of both LAMill and dry milling were calculated individually (shown in Fig. 17). Results showed that there was a 55% and 47.8% reduction of peak and mean principal cutting forces respectively by the proposed S&T controlled laser-heating method. The peak and mean feed force F_x were also decreased by 26.3% and 26.1% respectively. Consequently, the cutting power dropped off by 35.4%.

From the cutting force profiles in Fig. 16, the standard deviation of all cutting force components were also reduced by laser heating, which is good to obtain a better surface quality. This can be further verified by surface topography. To get the surface morphology, two areas (5mm×19mm) on the machined surface by LAMill and dry milling respectively were observed. S_a, S_z and S_q were selected as KPIs to show the roughness change of the machined surface due to laser heating. Results showed that the mean surface roughness S_a in dry milling and LAMill were 5.67 μm and 4.87μm respectively, and the maximum height S_z and root mean square height S_q decreased from 41.2 μm and 7.1 μm in dry

milling to 31.7 μm and 6.08 μm in LAMill respectively. This means that there is an at least 14% improvement in the surface roughness by using the proposed laser-heating method.

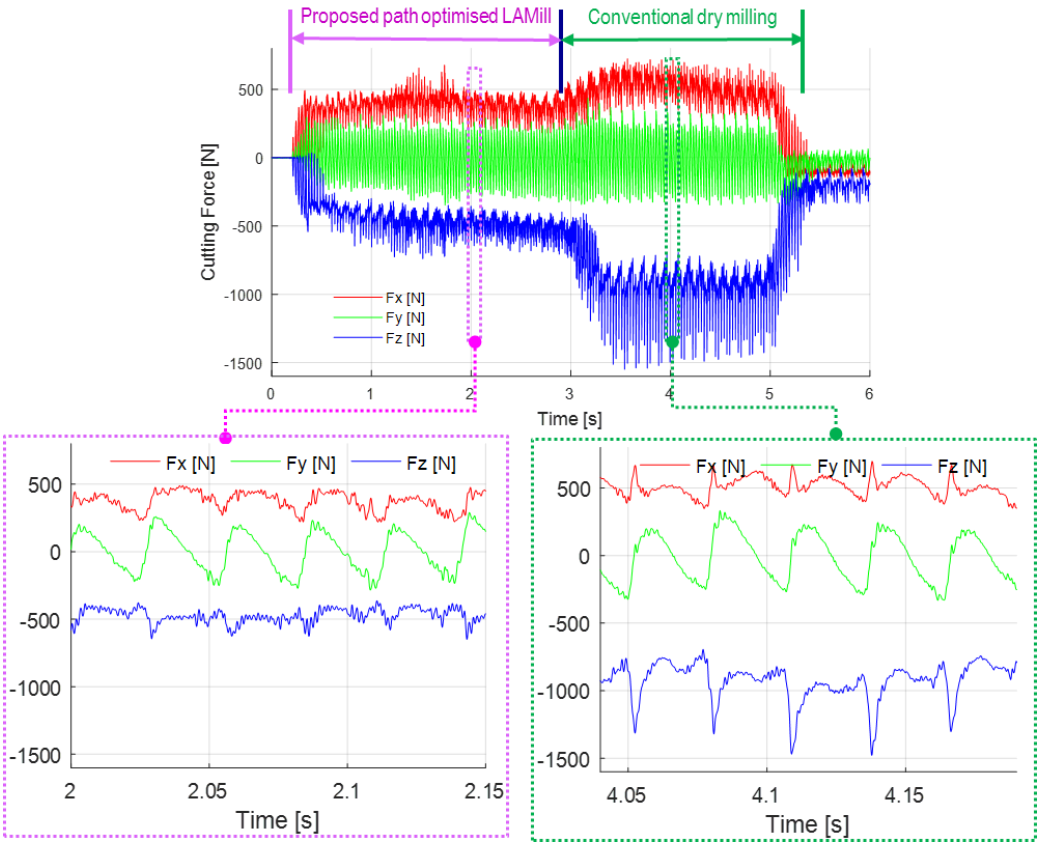

Fig. 16 Cutting forces of path-optimised LAMill

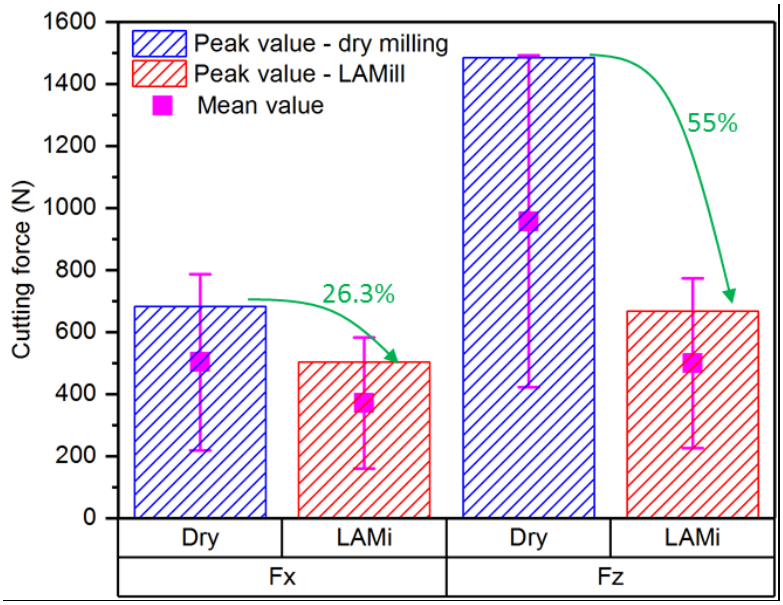

Fig. 17 Cutting force reduction in path-optimised LAMill: F_z and F_x reduced by 55% and 26.3% in peak value and 47.8% and 26.1% in mean value respectively

Subsurface microstructure was also investigated to further check the machining quality by path-optimised LAMill. The edged of the sample and centre area were observed because the side area is more likely to be overheated while the centre area tends to be heated insufficiently according to the modelling results

(as shown in in Fig. 8). As a comparison, microstructure at the same areas on the workpiece obtained by dry milling are presented in Fig. 18. It was found that HAZ which can cause the base material to change its phase was totally removed by the following milling process and no evident residual HAZ appeared. In addition, from Fig. 18 (a) and (b), both the edge area and the centre were heated well (without overheating or insufficient heating respectively). It is important to note that white layers and micro-cracks could be avoided by using the proposed laser-heating method (as compared in Fig. 18 (b) and (d)), which is essential to the part performance.

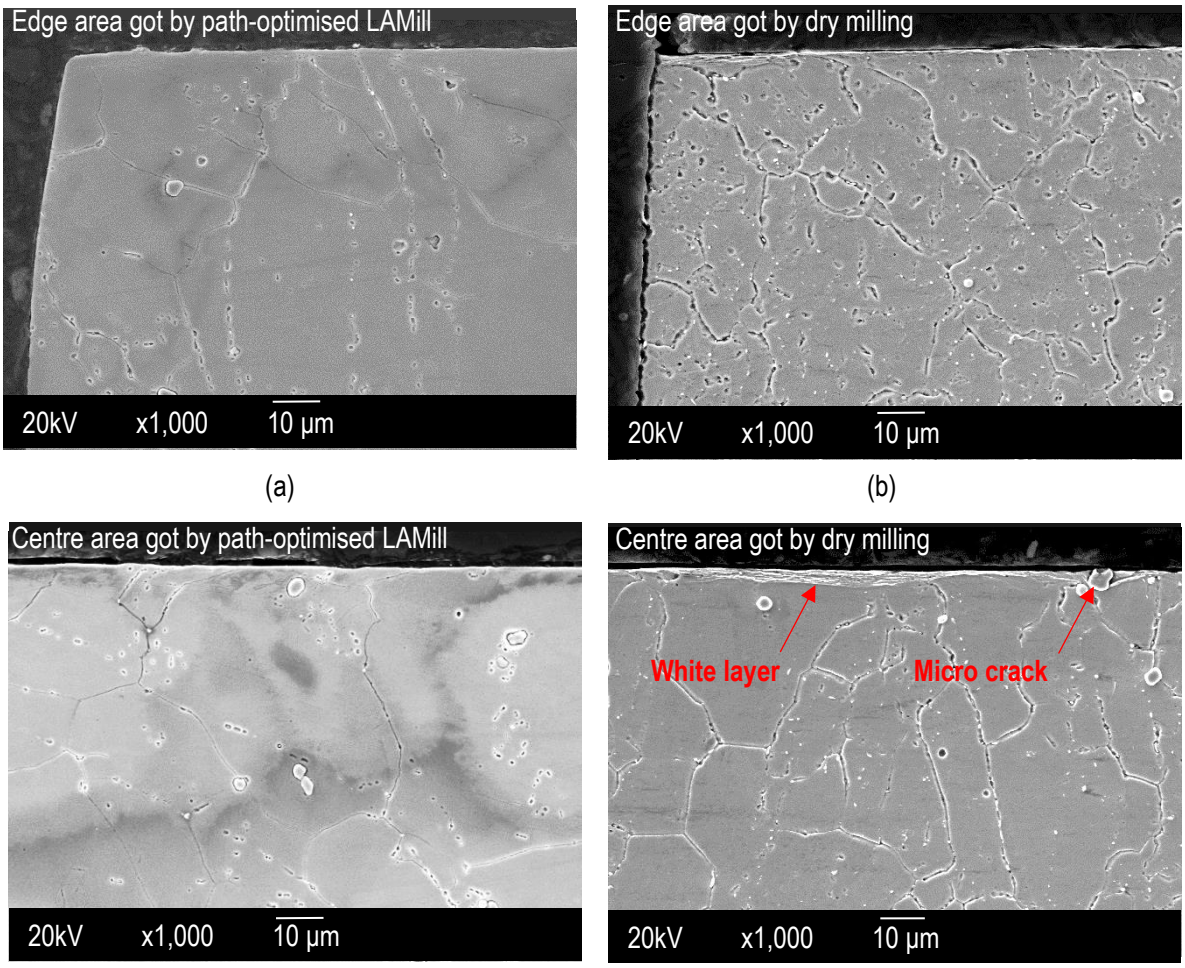

Fig. 18 Microstructure of path-optimised LAMill and dry milling subsurface: at edge area gotten by path-optimised LAMill (a) and dry milling (b), at center area gotten by path-optimised LAMill (c) and dry milling (d)

Through the above observations, the machining quality in path-optimised LAMill was kept the same if not better than the dry milling process while the principal cutting force dropped off by more than half. To further demonstrate the advantages of the our proposed S&T controlled laser-heating method, the conventional laser-heating method, where the laser spot is fixed with the cutting tool, was also implemented. A lower power (i.e. 3.6 kW) was employed in this test because the higher power would over burn the material severely. The conventional LAMill, path-optimised LAMill were conducted in successive and continuous order under the same laser power followed by the dry milling in one cutting pass and the results were shown in Fig. 19. Because the heating energy was concentrated around the

laser spot (Fig. 19 (e)) in the conventional heating method, the area nearby the laser spot was melted while the remaining area was not heated up sufficiently which results in a burned cutting surface and rarely decreased the cutting force (less than 17% reduction in mean principal cutting force). This can be seen from Fig. 19 (a) where the cutting force falls to zero when the insert engages with the laser heated area but remains the same when dry milling the remaining area. In addition, the non-homogeneous HAZ leads to a bad surface roughness (shown in Fig. 19 (h)).

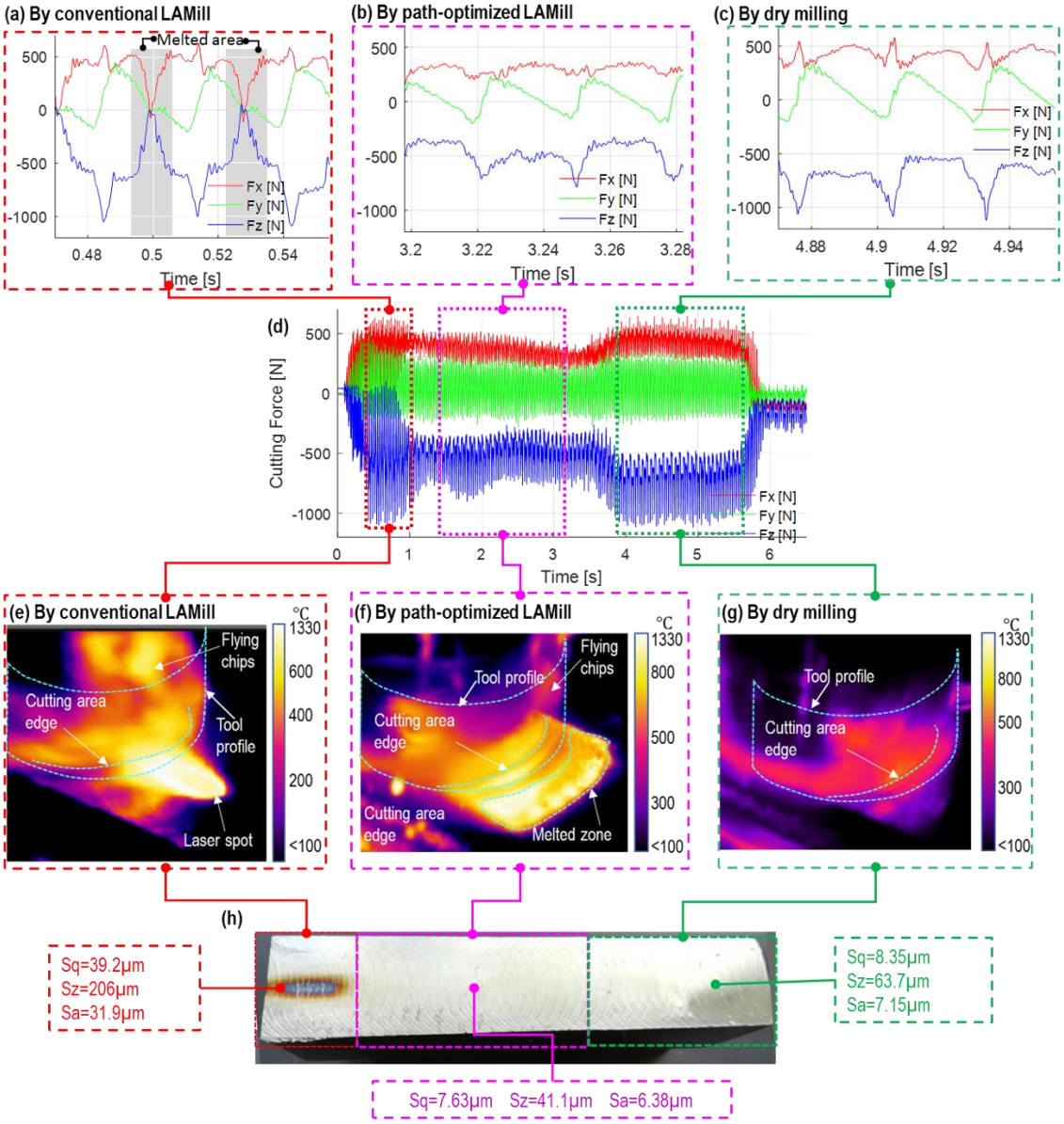

Fig. 19 Comparison of the conventional and S&T controlled laser-heating method: cutting forces in conventional LAMill were rarely decreased while the workpiece surface was burned

5 Conclusions

LAMill process is a promising method to significantly improve the machining productivity of difficult-to-cut materials. In the conventional approaches reported up to now, i.e. the conventional LAMill process, to soften the material before cutting, the laser beam is projected ahead of the cutting area at a fixed location relative to the cutting tool. However, the fixed laser beam leads to a series of restrictions on the application

of this process, for example on the cutting width, which must be comparable to the laser spot diameter and consequently, the optics system needs to be changed frequently to adapt to different cutting widths.

To overcome these difficulties, a novelty spatially and temporally controlled laser-heating method was put forward, in which the laser beam oscillates ahead of the cutting area along the longitudinal direction (perpendicular to the feed direction).

A 3D transient heat conduction model which can predict the temperature distribution caused by a freeform laser trajectory was built as the foundation of the inverse problem. The laser configuration for the desired temperature distribution was obtained by solving the inverse problem. The laser configuration was defined by laser beam power, trajectory and scanning speed and represented by a quadruplet (P, X_{bi}, Y_{bi}, t_i). To reduce the computational cost, the laser trajectory was designed to be periodic and so that just one period of the cycle was optimised. The laser power was optimised to a fixed value during the whole scanning to further reduce the optimization scale. Two methods were developed for solving the inverse problem: the first one is to optimize the laser scanning speed for a predefined scanning path while the second one is to optimize the laser scanning path for a fixed laser scanning speed. Good temperature distributions can be obtained by both methods according to our modelling results. This is the first report on a scientific approach to laser assisted milling, solved appropriately by addressing the inverse problem in heat placement.

The proposed S&T controlled laser-heating method was verified by experiments in two steps. The temperature distributions measured after scanning using the two trajectories obtained by the above two methods were verified in the first step. However, only the path-optimised trajectory was validated because the speed-optimised trajectory cannot be interpreted properly by the laser scanning system due to technical limitations of the galvanometer. The temperature distribution on the top surface was recorded by a thermal camera and the internal temperature was measured by a thermocouple array embedded inside the workpiece. Good agreement obtained between the shape of the HAZ on the top surface and the simulated temperature also matched well with the temperature logged by thermocouples (less than 10% errors in peak temperature). In the second step, the optimised laser heating trajectory was tested during the high feed milling process of Inconel 718. The results showed that the principal cutting force was reduced by 55% while the machining quality was better than that obtained using the conventional dry milling process.

To further demonstrate the advantages by the proposed S&T controlled laser-heating method, the conventional LAMill with a fixed laser spot was also conducted as a comparison. Results showed that cutting forces were hardly reduced and the workpiece surface was burned by the conventional laser-heating method, which is unacceptable for the performance of the machined part.

Our proposed S&T controlled laser heating method provides an efficient way to heat up an area far bigger than the laser spot size to the required temperature distribution. And the application scenarios of the method are very wide, such as any laser heating treatment, laser bending, 3D printing, etc. However, there are many questions still open regarding to the specific application cases. Take the LAMill demonstrated in our paper as an example, though the proposed S&T laser-heating method narrowed the

gap of the LAMill method between laboratory research and industrial applications, there are serval questions still need to be solved to further improve the LAMill process, such as the mechanics involved in the cutting force reduction and process optimization to control the workpiece surface integrity, as well as theoretical questions concerning the solution of the inverse problem and the paths obtained thereby. In addition, the comprehensive evaluation of the influences on the original process by introducing the laser should further be explored, such as the surface integrity, tool life, total machining cost, etc. for LAMill.

Acknowledgement

This project has received funding from the Clean Sky 2 Joint Undertaking under the European Union's Horizon 2020 research and innovation programme under grant agreement No. 754807. Our partners GKN Aerospace Sweden AB and SECO Tools AB are also acknowledged. The authors also would like to thank Jon Lambarri from IK4-TEKNIKER for his support on this work. The first author also gratefully appreciate the financial support from China Scholarship Council (CSC).

References

[1] C. Kuo, Y. Hsu, C. Chung, C.-C.A. Chen, Multiple criteria optimisation in coated abrasive grinding of titanium alloy using minimum quantity lubrication, International Journal of Machine Tools and Manufacture, 115 (2017) 47-59.

[2] Z. Liao, D. Axinte, M. Mieszala, R. M'Saoubi, J. Michler, M. Hardy, On the influence of gamma prime upon machining of advanced nickel based superalloy, Cirp Annals-Manufacturing Technology, 67 (2018) 109-112.

[3] O. Gavalda Diaz, D.A. Axinte, Towards understanding the cutting and fracture mechanism in Ceramic Matrix Composites, International Journal of Machine Tools and Manufacture, 118-119 (2017) 12-25.

[4] M.S. Dargusch, S. Sun, J.W. Kim, T. Li, P. Trimby, J. Cairney, Effect of tool wear evolution on chip formation during dry machining of Ti-6Al-4V alloy, International Journal of Machine Tools and Manufacture, 126 (2018) 13-17.

[5] A. Thakur, S. Gangopadhyay, State-of-the-art in surface integrity in machining of nickel-based super alloys, International Journal of Machine Tools and Manufacture, 100 (2016) 25-54.

[6] D. Gao, Z. Liao, Z.K. Lv, Y. Lu, Multi-scale statistical signal processing of cutting force in cutting tool condition monitoring, International Journal of Advanced Manufacturing Technology, 80 (2015) 1843-1853.

[7] E. Oezkaya, N. Beer, D. Biermann, Experimental studies and CFD simulation of the internal cooling conditions when drilling Inconel 718, International Journal of Machine Tools and Manufacture, 108 (2016) 52-65.

[8] X. Zhang, G.L. Tnay, K. Liu, A.S. Kumar, Effect of apex offset inconsistency on hole straightness deviation in deep hole gun drilling of Inconel 718, International Journal of Machine Tools and Manufacture, 125 (2018) 123-132.

[9] Z. Liao, D. Gao, Y. Lu, Z.K. Lv, Multi-scale hybrid HMM for tool wear condition monitoring, International Journal of Advanced Manufacturing Technology, 84 (2016) 2437-2448.

[10] C.-M. Lee, W.-S. Woo, J.-T. Baek, E.-J. Kim, Laser and arc manufacturing processes: A review, International Journal of Precision Engineering and Manufacturing, 17 (2016) 973-985.

[11] O. Shams, A. Pramanik, T. Chandratilleke, Thermal-Assisted Machining of Titanium Alloys, in: Advanced Manufacturing Technologies, Springer, 2017, pp. 49-76.

[12] M. Brandt, S. Sun, Laser Assisted Machining : Current Status and Future Scope, in: Laser-Assisted Fabrication of Materials, 2013, pp. 113-157.

[13] R.A.R. Rashid, S. Sun, G. Wang, M.S. Dargusch, An investigation of cutting forces and cutting temperatures during laser-assisted machining of the Ti-6Cr-5Mo-5V-4Al beta titanium alloy, International Journal of Machine Tools & Manufacture, 63 (2012) 58-69.

[14] Garcí, V. a Navas, I. Arriola, O. Gonzalo, J. Leunda, Mechanisms involved in the improvement of Inconel 718 machinability by laser assisted machining (LAM), International Journal of Machine Tools and Manufacture, 74 (2013) 19-28.

[15] J.W. Ahn, W.S. Woo, C.M. Lee, A study on the energy efficiency of specific cutting energy in laser-assisted machining, Applied Thermal Engineering, 94 (2016) 748-753.

[16] M. Anderson, R. Patwa, Y.C. Shin, Laser-assisted machining of Inconel 718 with an economic analysis, International Journal of Machine Tools & Manufacture, 46 (2006) 1879-1891.

[17] P. Dumitrescu, P. Koshy, J. Stenekes, M. Elbestawi, High-power diode laser assisted hard turning of AISI D2 tool steel, International Journal of Machine Tools and Manufacture, 46 (2006) 2009-2016.

[18] C.R. Dandekar, Y.C. Shin, J. Barnes, Machinability improvement of titanium alloy (Ti–6Al–4V) via LAM and hybrid machining, International Journal of Machine Tools and Manufacture, 50 (2010) 174-182.

[19] K. Venkatesan, The study on force, surface integrity, tool life and chip on laser assisted machining of inconel 718 using Nd: YAG laser source, Journal of Advanced Research, 8 (2017) 407-423.

[20] X. Kong, L. Yang, H. Zhang, G. Chi, Y. Wang, Optimization of surface roughness in laser-assisted machining of metal matrix composites using Taguchi method, The International Journal of Advanced Manufacturing Technology, 89 (2017) 529-542.

[21] F.M. Guenael Germain, Jean Lu Lebrun, Anne Morel, Bertrand Huneau, Effect of laser assistance machining on residual stress and fatigue strength for a bearing steel (100Cr6) and a titanium alloy (Ti 6Al 4V), Materials Science Forum, 524-525 (2006).

[22] G. Germain, P. Dal Santo, J.L. Lebrun, Comprehension of chip formation in laser assisted machining, International Journal of Machine Tools and Manufacture, 51 (2011) 230-238.

[23] P.A. Rebro, Y.C. Shin, F.P. Incropera, Design of operating conditions for crackfree laser-assisted machining of mullite, International Journal of Machine Tools and Manufacture, 44 (2004) 677-694.

[24] F. Zhao, W.Z. Bernstein, G. Naik, G.J. Cheng, Environmental assessment of laser assisted manufacturing: case studies on laser shock peening and laser assisted turning, Journal of Cleaner Production, 18 (2010) 1311-1319.

[25] G. Chryssolouris, N. Anifantis, S. Karagiannis, Laser assisted machining: An overview, Journal of Manufacturing Science and Engineering-Transactions of the Asme, 119 (1997) 766-769.

[26] B. Yang, S. Lei, Laser-Assisted Milling of silicon nitride ceramic, International Journal of Mechatronics and Manufacturing Systems, 1 (2008) 15.

[27] Y. Tian, B. Wu, M. Anderson, Y.C. Shin, Laser-Assisted Milling of Silicon Nitride Ceramics and Inconel 718, Journal of Manufacturing Science and Engineering, 130 (2008) 031013.

[28] C. Brecher, M. Emonts, C.J. Rosen, J.P. Hermani, Laser-assisted Milling of Advanced Materials, Lasers in Manufacturing 2011: Proceedings of the Sixth International Wlt Conference on Lasers in Manufacturing, Vol 12, Pt A, 12 (2011) 599-606.

[29] Z. Pan, Y. Feng, T.-P. Hung, Y.-C. Jiang, F.-C. Hsu, L.-T. Wu, C.-F. Lin, Y.-C. Lu, S.Y. Liang, Heat affected zone in the laser-assisted milling of Inconel 718, Journal of Manufacturing Processes, 30 (2017) 141-147.

[30] M. Bermingham, W. Sim, D. Kent, S. Gardiner, M. Dargusch, Tool life and wear mechanisms in laser assisted milling Ti–6Al–4V, Wear, 322 (2015) 151-163.

[31] K.S. Kim, T.W. Kim, C.M. Lee, Analysis of a laser assisted milling process with inclination angles, International Journal of Precision Engineering & Manufacturing, 14 (2013) 1495-1499.

[32] R. Singh, M.J. Alberts, S.N. Melkote, Characterization and prediction of the heat-affected zone in a laser-assisted mechanical micromachining process, International Journal of Machine Tools and Manufacture, 48 (2008) 994-1004.

[33] D. Kang, C. Lee, A study on the development of the laser-assisted milling process and a related constitutive equation for silicon nitride, CIRP Annals-Manufacturing Technology, 63 (2014) 109-112.

[34] M.J. Bermingham, P. Schaffarzyk, S. Palanisamy, M.S. Dargusch, Laser-assisted milling strategies with different cutting tool paths, International Journal of Advanced Manufacturing Technology, 74 (2014) 1487-1494.

[35] M.M. Kashani, M.R. Movahhedy, M.T. Ahmadian, R.S. Razavi, Analytical Solution of Transient Three-Dimensional Temperature Field in a Rotating Cylinder Subject to a Localized Laser Beam, Journal of Heat Transfer, 139 (2017) 062701.

[36] H. Roostaei, M.R. Movahhedy, Analysis of Heat Transfer in Laser Assisted Machining of Slip Cast Fused Silica Ceramics, Procedia CIRP, 46 (2016) 571-574.

[37] H.G. Woo, H.S. Cho, Three-dimensional temperature distribution in laser surface hardening processes, Proceedings of the Institution of Mechanical Engineers Part B-Journal of Engineering Manufacture, 213 (1999) 695-712.

[38] M. Van Elsen, M. Baelmans, P. Mercelis, J.P. Kruth, Solutions for modelling moving heat sources in a semi-infinite medium and applications to laser material processing, International Journal of Heat and Mass Transfer, 50 (2007) 4872-4882.

[39] M. Kubiak, W. Piekarska, S. Stano, Modelling of laser beam heat source based on experimental research of Yb:YAG laser power distribution, International Journal of Heat and Mass Transfer, 83 (2015) 679-689.

[40] G. Araya, G. Gutierrez, Analytical solution for a transient, three-dimensional temperature distribution due to a moving laser beam, International Journal of Heat and Mass Transfer, 49 (2006) 4124-4131.

[41] D.H. Kim, C.M. Lee, A study of cutting force and preheating-temperature prediction for laser-assisted milling of Inconel 718 and AISI 1045 steel, International Journal of Heat & Mass Transfer, 71 (2014) 264-274.

[42] H.T. Ding, N.G. Shen, Y.C. Shin, Thermal and mechanical modeling analysis of laser-assisted micro-milling of difficult-to-machine alloys, Journal of Materials Processing Technology, 212 (2012) 601-613.

[43] K.D. Cole, J.V. Beck, A. Haji-Sheikh, B. Litkouhi, Heat conduction using Green's functions, Taylor & Francis, 2010.

[44] Special metals technical bulletin: Inconel 718, in, http://www.specialmetals.com/tech-center/alloys.html.

[45] P. Mignanelli, N. Jones, M. Hardy, H. Stone, On the Time-Temperature-Transformation Behavior of a New Dual-Superlattice Nickel-Based Superalloy, Metallurgical and Materials Transactions A, (2017) 1-9.

[46] J. Diaz-Alvarez, A. Tapetado, C. Vazquez, H. Miguelez, Temperature Measurement and Numerical Prediction in Machining Inconel 718, Sensors (Basel), 17 (2017).

Appendix: forward problem derivation

The solution of forward heat conduction problem, which is the temperature distribution for a given laser configuration, will be derived in this section. The temperature distribution in the workpiece during the LAMill process can be described by the three-dimension transient heat conduction equation shown in Eq. (1) [43], in which all material property parameters (e.g. density, thermal conductivity) were treated as constant to simplify the problem [16]. We reproduce this here as

$$\frac{\partial^2\theta}{\partial x^2}+\frac{\partial^2\theta}{\partial y^2}+\frac{\partial^2\theta}{\partial z^2}+\frac{1}{k}q'''(x,y,z,t)=\frac{1}{\alpha}\frac{\partial\theta}{\partial t} \tag{A1}$$

The heat flux of a TEM00 mode laser beam can be modelled by a Gaussian distribution function [39] as

$$q'''(x,y,z,t)=q_0\exp\left(-\frac{\big(x-x_b(t)\big)^2}{r_{bx}^2}\right)\exp\left(-\frac{\big(y-y_b(t)\big)^2}{r_{by}^2}\right)\delta(Z) \tag{A2}$$

Because the laser head is usually fixed on the spindle and the laser beam is focused before machining, the depth of the cut can change the actual size of the laser spot. The new laser spot radius can be evaluated by Eq.(A3), in which z_R is the Rayleigh length of the laser beam. However, noting that a_p in LAMill is usually very small (i.e. 0.26mm) compared to z_R (i.e. 20.5mm for our laser system), the size change of the beam would be negligible (i.e. 0.008% in our case).

$$r_{be}=r_b\sqrt{1+\left(\frac{a_p}{z_R}\right)^2} \tag{A3}$$

The heat affected zone is usually small compared to the workpiece size and hence the workpiece can be treated as semi-infinite in the z direction and infinite in the x and y directions. Furthermore, because heat losses on the surface are small compared to the laser heat absorbed by the workpiece, the convective and radiative heat losses at the upper surface are ignored and the upper surface is treated as adiabatic, and at the initial time , the workpiece is in heat equilibrium with the ambient environment so we have

$$\left.\frac{\partial\theta}{\partial z}\right|_{z=0}=0 \tag{A4}$$

$$\theta(x,y,z,0)=0 \tag{A5}$$

The Green's function (GF) method is a powerful tool for solving linear heat conduction problems, in which the GF can be interpreted as the temperature distribution corresponding to an impulsive heat source [43]. The Green's function corresponding to the above initial and boundary conditions is

$$G(x,y,z,t|x',y',z',\tau)=\frac{2}{\big(4\pi\alpha(t-\tau)\big)^{\frac{3}{2}}}\exp\left(-\frac{|\mathbf{x}-\mathbf{x}'|^2}{4\alpha(t-\tau)}\right) \tag{A6}$$

with $\mathbf{x}=(x,y,z)$, $\mathbf{x}'=(x',y',z')$ and $|\mathbf{x}-\mathbf{x}'|=\sqrt{(x-x')^2+(y-y')^2+(z-z')^2}$.

There are two physical interpretations of Green's function. The first one is that a Green's function is the temperature distribution caused by a particular initial condition and the second interpretation is the temperature distribution for an instantaneous heat source. Thus the temperature distribution caused by the laser beam in LAMill can be obtained by the following integral:

$$\theta(x,y,z,t) = \frac{\alpha}{k}\int_{\tau=0}^{t}\int_{x'=-\infty}^{\infty}\int_{y'=-\infty}^{\infty}\int_{z'=-\infty}^{0} G(x,y,z,t|x',y',z',\tau)q'''(x',y',z',\tau)dx'dy'dz'd\tau \tag{A7}$$

Performing the spatial integration analytically leads to the final form of the temperature distribution,

$$\begin{aligned}\theta(x,y,z,t) = \frac{2\alpha}{k}q_0 \int_{\tau=0}^{t} & \frac{1}{\left(4\pi\alpha(t-\tau)\right)^{\frac{3}{2}}} \frac{4\pi}{\sqrt{\frac{4}{r_{bx}^2}+\frac{1}{\alpha(t-\tau)}}\sqrt{\frac{4}{r_{by}^2}+\frac{1}{\alpha(t-\tau)}}} \\ & \times \exp\left(-\frac{\left(x-x_b(\tau)\right)^2}{r_{bx}^2+4\alpha(t-\tau)}\right)\times\exp\left(-\frac{\left(y-y_b(\tau)\right)^2}{r_{by}^2+4\alpha(t-\tau)}\right) \\ & \times \exp\left(-\frac{z^2}{4\alpha(t-\tau)}\right)d\tau\end{aligned} \tag{A8}$$